Chapter 22
Hybrid Membrane-Type Fuel Cells for Intermediate Temperatures

Toshinobu Yogo

Abstract This chapter describes the syntheses and characterization of proton-conductive hybrid membranes for the use at intermediate temperatures from 100 to 150 °C. The inorganic–organic hybrid membranes were synthesized from an unsaturated organoalkoxysilane and a vinylphosphonic acid derivative via copolymerization and acidic hydrolysis. The hybrid membranes were characterized by infrared spectroscopy, thermogravimetry, and indentation test. The proton conductivity was measured for various compositions of the membranes. The current–voltage curves for the membrane electrode assembly consisting of the hybrid membrane were evaluated.

Keywords PEFC · Inorganic–organic hybrid · Sol–gel process · Copolymerization · Conductivity · Fuel cells

22.1 Introduction

Polymer electrolyte fuel cells (PEFCs) are characterized by their high energy-conversion efficiency and clean exhaust gas [1, 2]. Perfluorosulfonic polymers are the representatives of PEFCs, and have high proton conductivity, high mechanical strength, and good chemical stability. However, these membranes exhibit the maximum performance at around 80 °C and 100% relative humidity (RH). Perfluorosulfonic polymers require a complicated water management system in order to maintain high relative humidity and pure hydrogen gas with low inclusion of CO less than 20 ppm to avoid the poisoning of Pt anode catalysts [3]. When the operation temperature of PEFCs is raised to higher temperatures around 130 °C, the greatest advantages, such as a decrease in catalyst poisoning, higher efficiency, and a simple management system, are achieved [4, 5]. Therefore,

T. Yogo (✉)
Institute of Materials and Systems for Sustainability, Nagoya University, Nagoya, Japan
e-mail: yogo@imass.nagoya-u.ac.jp

Y. Setsuhara et al. (eds.), *Novel Structured Metallic and Inorganic Materials*, https://doi.org/10.1007/978-981-13-7611-5_22

proton-conducting materials with high conductivity at intermediate temperatures from 100 to 150 °C are required.

Inorganic–organic hybrid materials are nanocomposites between organics and inorganics. Organic materials have merits of flexibility and chemical functionality, whereas inorganic materials have advantages of high mechanical strength, chemical, and thermal stability. Thus, the demerits of organic materials, such as low thermal and mechanical stability, can be improved by the incorporation of inorganic materials. As silica and/or organosiloxane form a network structure, silica-based inorganic–organic hybrids are appropriate materials for the proton-conductive membranes at intermediate temperatures [6–19]. Only mixing and doping of proton carriers in silica and/or organosiloxane matrix is not desirable for the synthesis of proton-conductive membranes. As the proton carriers, such as sulfonic acid, phosphonic acid, are quite soluble in water, which is generated during fuel cell reaction, the proton carriers are leached out from the membrane during use [20]. The leach-out of the carriers results in the decrease in conductivity and degradation of cell performance. Therefore, the proton carriers should be bound to the matrix polymer via covalent bonds.

22.2 Proton Conduction in the PEFC Membranes

Figure 22.1 shows the schematic principle of the H_2–O_2 fuel cell. The fuel cell consists of membrane sandwiched with two electrodes, anode and cathode. The membrane should have a very high proton conductivity but is not permeable to gas.

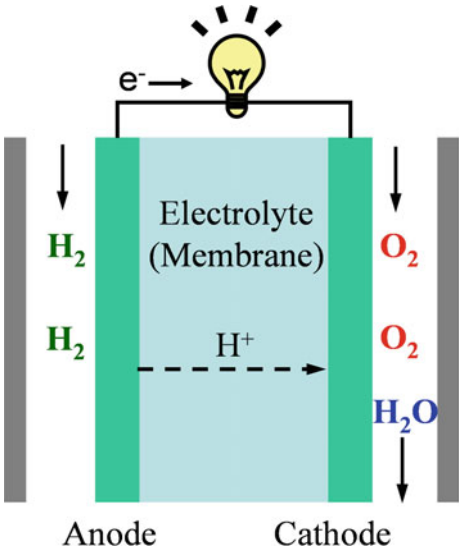

Fig. 22.1 Basic principle of H_2–O_2 fuel cell

At the anode, hydrogen is reduced electrochemically to protons according to Eq. (22.1).

$$H_2 \rightarrow 2H^+ + 2e^- \tag{22.1}$$

The generated protons enter the membrane and move to the cathode, whereas the generated electrons collected by the metallic electrode. At the cathode, the protons are electrochemically reacted with oxygen, producing water (Eq. (22.2)).

$$\frac{1}{2}O + 2H^+ + 2e^- \rightarrow H_2O \tag{22.2}$$

Thus, the overall reaction is the formation of water from 1 mol of hydrogen and a half mole of oxygen (Eq. (22.3)).

$$H_2 + \frac{1}{2}O_2 \rightarrow H_2O \tag{22.3}$$

The electromotive force or reversible potential E° at the standard state generated by Eq. (22.3) is represented by the following equation:

$$E^\circ = -\Delta G^\circ / nF \tag{22.4}$$

where ΔG° is the standard free energy change, n is the number of moles of electrons involved, and F is Faraday's constant. The value of ΔG accompanied by Eq. (22.3) is −229 kJ/mole, n = 2, F = 96,500 C/g mole electron, and therefore the value of E is 1.23 V.

Although fuel cells consist of various parts, such as membrane, electrodes, catalyst, H_2, and O_2 gas supplies, the membrane is a key material for the successful operation of cells at intermediate temperatures. The membranes are required to have high proton conductivity, unpermeability to hydrogen and oxygen, non-electronic conductivity, high chemical and electrochemical stability, high mechanical strength, and high thermal stability.

22.3 Synthesis of Siloxane-Based Hybrid Materials

The present hybrid material is composed of an organic main chain and inorganic Si–O linkage. The organic chain is formed via radical polymerization of the unsaturated double bond, while the Si–O linkage is constructed via sol–gel condensation of silicon alkoxide.

The hydrolysis of silicon alkoxide is a typical sol–gel reaction, and proceeds under both acidic and basic conditions [21]. Base-catalyzed reactions occur by nucleophilic substitution. Not only the electron density around the central silicon atom, but also the steric effects derived from the size of substituent groups influence

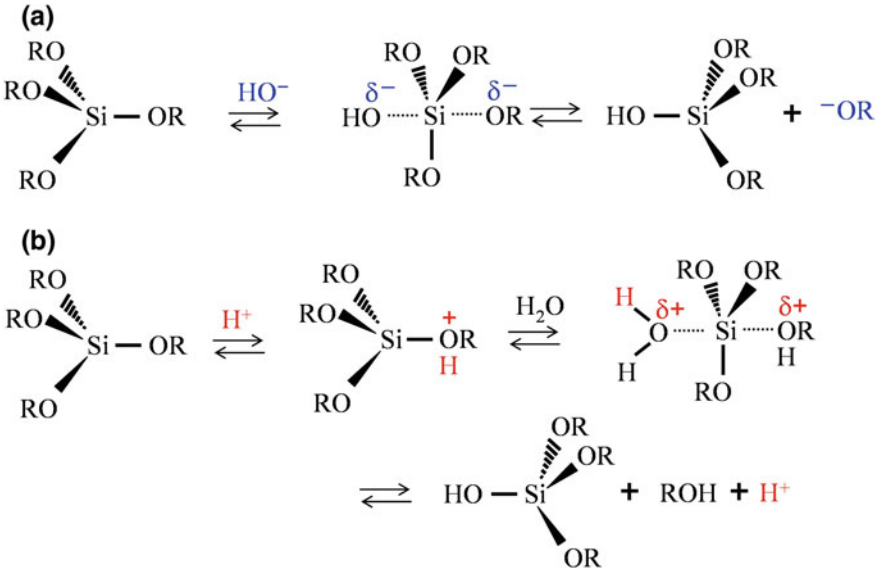

Fig. 22.2 Hydrolysis of silicon alkoxide, **a** hydrolysis under basic conditions, **b** hydrolysis under acidic conditions

the easiness of the nucleophilic attack by HO^-. As the reaction rate decreases with an increase in bulk and basic alkoxy groups around the central silicon atom, the basic hydrolysis undergoes through S_N2 mechanism with inversion of the silicon tetrahedron as shown in Fig. 22.2a. On the other hand, under acidic conditions, an alkoxy group is protonated, withdrawing electron density from silicon (Fig. 22.2b). Thus, the central silicon is more susceptible to electrophilic attack by H_2O. The backside attack of water to the central silicon inverts the silicon tetrahedron. Hence, the less sterically crowding substituent around silicon enhances the acidic hydrolysis rate.

The hydrolysis of the Si–OR bond results in the formation of unstable silanols (Si–OH) that condensate yielding the Si–O–Si linkage. On the other hand, Si–C bond is stable to hydrolysis, and intact during sol–gel reaction. These reactions are shown in the following Eqs. (22.5) and (22.6). As the Si–C bond is stable during sol–gel condensation, T linkage is formed from $RSi(OR')_3$.

$$RSi(OR')_3 + 3H_2O \rightarrow RSi(OH)_3 + 3R'OH \tag{22.5}$$

$$nRSi\,(OH)_3 \rightarrow RSi(O-)_3 \tag{22.6}$$

In T^n notation, T corresponds to a silicon atom bonded to three oxygen atoms forming tetrahedron. The superscript n indicates the number of other T unit attached to the $RSiO_3$ tetrahedron as shown in Fig. 22.3.

The organic–inorganic hybrid for fuel cells consist of the building blocks of inorganic Si–O–Si linkage covalently bonded to the organic polymer chain.

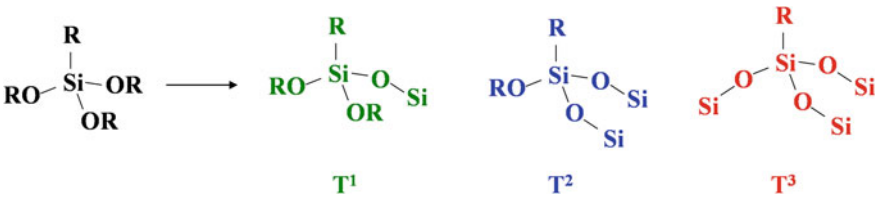

Fig. 22.3 T^3 notation of $RSiO_3$ tetrahedra

Generally, inorganic–organic hybrid is classified into two groups according to the character of the chemical bonds between organic and inorganic phase [22]. Figure 22.4 shows the schematic structures of Class I type and Class II type hybrids. The tetrahedron and the flat hexagon correspond to an inorganic and an organic unit, respectively. The Class I type hybrids consist of organic and inorganic phases, which are linked together through weak bonds, such as van der Waals force, hydrogen bonding, and weak electrostatic interactions. On the other hand, in Class II-type hybrids, an inorganic component is bound with an organic component through strong covalent chemical bonds. Therefore, Class II-type hybrids are much more appropriate for the membranes, in which proton carriers are fixed firmly to the stable inorganic–organic hybrid matrices via chemical bonds, leading to the prevention of the leach-out problem.

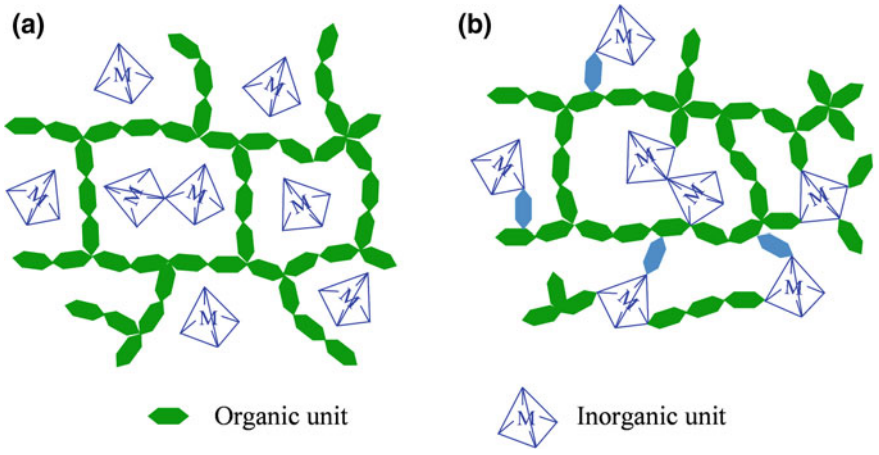

Fig. 22.4 Schematic structures of the hybrid material, **a** Class I-type hybrid, **b** Class II-type hybrid

22.4 Synthesis of Inorganic–Organic Hybrid Membrane

Figure 22.5 shows the starting materials and the reaction scheme for the synthesis of hybrid membrane. 4-fluorophenylvinylphosphonic acid (FC_6H_4PVA) consists of a vinyl group for radical polymerization and a phosphonic acid as a proton carrier. (Trimethoxysilylmethyl)styrene (TMSMS) includes a vinyl group for polymerization and trimethoxysilyl groups for hydrolysis and condensation. TMSMS was copolymerized with FC_6H_4PVA in dimethylformamide (DMF) with various monomer ratios in the presence of AIBN initiator. The samples were named as x/y = TMSMS/FC_6H_4VPA, more specifically, Si/P, according to their molar ratios. After the sealed glass capsule was heated at 85 °C for 8 h, a viscous solid copolymer was separated by centrifuging. The TMSMS–FC_6H_4VPA copolymer was dissolved in anhydrous DMF again immediately after separation. Then, 1.0 N hydrochloric acid solution was added dropwise to the copolymer solution to hydrolyze silicon alkoxide. The solution was stirred at room temperature for 24 h, yielding a sol, and the sol obtained was casted onto a Teflon plate. The casted film was heated in a dry oven at a stepwise heat treatment from 100 to 140 °C. The synthesized hybrid is classified to Class II hybrid, because the organic polymer chain is covalently bound to the Si–O linkages. The representative photographs of the hybrid membrane are shown in Fig. 22.6. The membranes are transparent and flexible. The optical transparency indicates that the membrane includes no

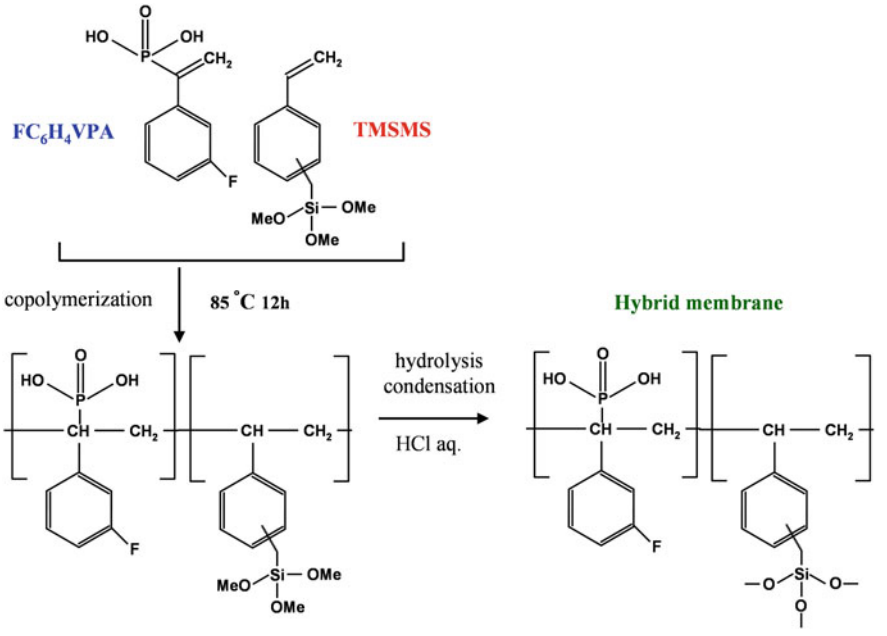

Fig. 22.5 Reaction procedure for the synthesis of hybrid membrane

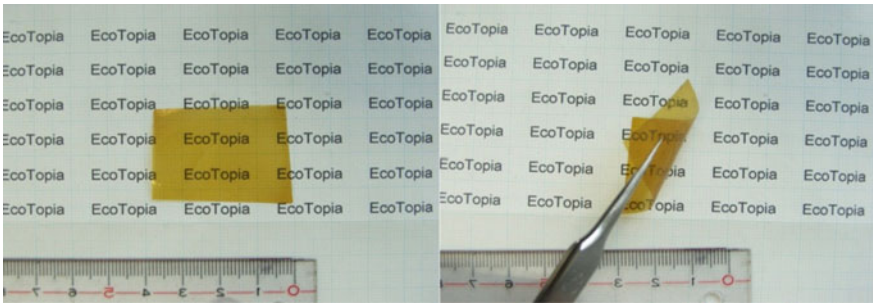

Fig. 22.6 Photographs of the hybrid membranes (Si/P = 1/6)

micron-sized region as the origin of light scattering. The flexibility is required for the construction of membrane electrode assembly (MEA) for fuel cell measurement.

TMSMS, FC_6H_4VPA, and the hybrid membrane with Si/P ratios of 1/2, 1/4, and 1/6 were analyzed by IR spectroscopy. TMSMS exhibited a C=C stretching band at 1630 cm^{-1}, aromatic bands at 1590, and 1490 cm^{-1}, and a Si–OCH_3 band at 827 cm^{-1} [23]. The P–OH bands were observed for FC_6H_4VPA as broad absorption bands from 2300 to 2800 cm^{-1}. Moreover, FC_6H_4VPA showed the absorption bands at 1583 and 1490 cm^{-1} attributed to the aromatic ring, the C=C and C–F stretching absorptions at 1620 and 1200 cm^{-1}, respectively. After copolymerization between TMSMS and FC_6H_4VPA followed by hydrolysis, the C=C absorption disappeared. In addition, the Si–OCH_3 band of TMSMS at 827 cm^{-1} disappeared in the spectra of all of the hybrid membranes, and a new absorption band for the Si–O–Si bond appeared at 1110 cm^{-1}. From these results, the hybrid was synthesized via the copolymerization of C=C bonds and the hydrolysis condensation of Si–OCH_3 groups.

Figure 22.7 shows the ^{29}Si CP-MAS NMR spectra of the hybrid membranes with Si/P ratios of 1/2, 1/4, and 1/6. Two signals were observed at −60 and −71 ppm in the T region which are assigned to T^2 and T^3, respectively [24]. Three-dimensional Si–O–Si cross-linkage is formed in the hybrid membranes through the hydrolysis and condensation of the Si–OCH_3 groups. Moreover, when the Si/P ratio decreases from 1/2 to 1/6, the intensity of the T^2 signal decreases. These results indicate that three-dimensional cross-links form more easily in the membranes with high P contents. Hence, the Si–OCH_3 groups of TMSMS undergo more rapid and complete hydrolysis, leading to the exclusive formation of T^3 cross-linkages, when the FC_6H_4VPA content is high. As phosphonic acid promotes the effective acidic condensation of the Si–OCH_3 bonds, the formation of T^3 linkages is more favorable than that of T^2 linkages.

The thermogravimetric curves were measured for the TMSMS/FC_6H_4VPA hybrid membranes with Si/P ratios of 1/2, 1/4, and 1/6 under an O_2 flow from room temperature to 800 °C. The gradual weight losses below 8 wt% were observed for all the membranes up to 180 °C. The weight loss was ascribed to the desorption of physically absorbed water. No other weight change was observed for the

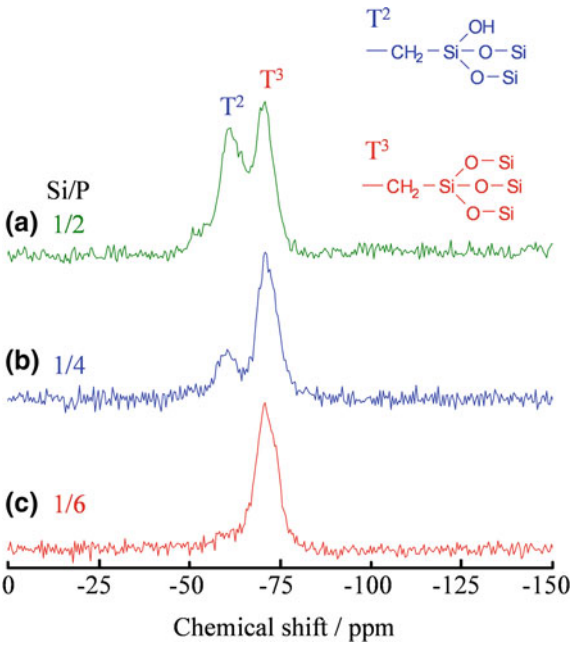

Fig. 22.7 ^{29}Si NMR spectra of hybrid membranes with the ratios of Si/P = **a** 1/2, **b** 1/4, **c** 1/6. Reprinted from Ref. [18]. Copyright 2015, with permission from Elsevier

membranes up to 180 °C. Therefore, the hybrid membranes were found to be thermally stable up to 180 °C, which is the higher temperature than the targeted temperature from 100 to 150 °C.

The oxidative stability of the TMSMS/FC_6H_4VPA membranes was examined using Fenton's reagent [8]. After treatment in Fenton's reagent at 80 °C for 24 h, the membranes with Si/P ratios of 1/4 and 1/6 maintained their outer shapes with no visible cracks. Usually, all organic polymer membranes dissolved in Fenton's reagent under the same conditions [25, 26]. Therefore, the chemical stability of the hybrid membranes is confirmed for fuel cell applications.

The mechanical properties of the TMSMS/FC_6H_4VPA membranes were measured using a Knoop indentation test. The Knoop microhardness (μHK) were 0.18, 0.12, and 0.088 GPa for the TMSMS/FC_6H_4VPA membranes of 1/2, 1/4, and 1/6, respectively. The μHK value decreases with increasing FC_6H_4VPA amount from 1/2 to 1/6. This result indicates that the Si–O linkage contributes to the hardness of hybrid membranes. The elastic modulus (E) were 1.9, 1.8, and 1.9 GPa for the TMSMS/FC_6H_4VPA membranes of 1/2, 1/4, and 1/6, respectively. The μHK and E values for the membranes with TMSMS/FC_6H_4VPA = 1/2 and 1/4 were comparable to those for the polycarbonate (μHK (micro-Vickers hardness): 0.14 GPa; E: 2.3 GPa) [27]. The TMSMS/FC_6H_4VPA membrane with a Si/P ratio of 1/6 had a μHK value of 0.088 GPa and an E value of 1.9 GPa due to the high organic polymer content and large number of T^3 Si–O–Si linkages. The organic polymer chain does not contribute to the hardness, but to the E value. The Si NMR spectra (Fig. 22.7) revealed that the TMSMS/FC_6H_4VPA = 1/6 membrane includes the

highest amount of T^3 linkage, indicating that T^3-type linkages were more favorable than T^2-type linkages for strengthening the hybrids. The TMSMS/FC_6H_4VPA = 1/6 membrane consisting of only T^3 Si–O–Si linkages has the optimum flexibility, which is useful for the construction of MEAs, as shown Fig. 22.10.

22.5 Proton Conductivity and Fuel Cell Properties of the Membrane

Figure 22.8 shows the temperature dependence of the proton conductivity for the hybrid membranes synthesized with TMSMS/FC_6H_4VPA ratios of 1/2, 1/4, and 1/6 at various RH. The open and solid symbols represent the conductivities of the membranes at 100% RH and low humidities from 19.3% to 27.0% RH, respectively. The conductivity at each humidity level increased with increasing temperature up to 130 °C. In addition, the conductivity depends on the Si/P ratio, and the highest conductivity was observed for the membranes with the Si/P ratio of 1/6 at all humidities. The maximum conductivity of 6.4×10^{-2} S cm^{-1} was observed for the membrane with Si/P = 1/6 ratio at 130 °C and 100% RH. This result indicates that the conductivity increased with increasing phosphonic acid, which acts as the proton carrier. At a low humidity of ~20% RH, the conductivity of the present membrane at 80 °C (5.0×10^{-5} S cm^{-1}) is much higher than that of an alkoxyphenylsilane-phosphonic acid system (~1×10^{-6} S cm^{-1}) [28].

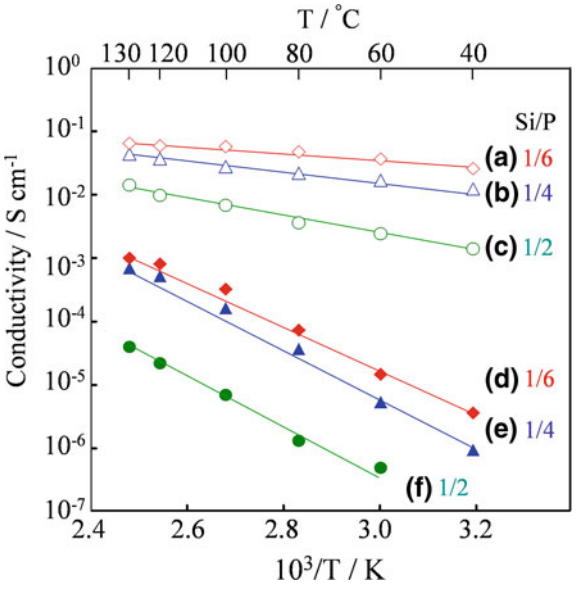

Fig. 22.8 Temperature dependences of the proton conductivities of hybrid membranes of TMSMS/FC_6H_4VPA with the ratios of 1/2, 1/4, and 1/6, **a** 1/6 at 100% RH, **b** 1/4 at 100% RH, **c** 1/2 at 100% RH, **d** 1/6 from 27.0 to 19.2% RH, **e** 1/4 from 27.0 to 19.2% RH, **f** 1/2 from 24.0 to 19.2% RH. Reprinted from Ref. [18]. Copyright 2015, with permission from Elsevier

As the proton conductivity increase with temperature, the conduction is thermally stimulated process. Therefore, the activation energies (Ea) for the proton conductivities at each humidity were calculated using the Arrhenius Eq. (22.7)

$$\ln \sigma = \ln A - Ea/kT \tag{22.7}$$

where A is the pre-exponential term, Ea is activation energy, and k is the Boltzmann constant. At 100% RH, the Ea values for the hybrid membranes with Si/P ratios of 1/2, 1/4, and 1/6 were determined to be 28, 15, and 11 kJ/mol, respectively. The Ea values for the membranes with Si/P ratios of 1/4 and 1/6 Si/P ratios were nearly the same as that of Nafion (9–13 kJ/mol) [29] Furthermore, at low RH, the Ea values for the membranes with Si/P ratio of 1/2, 1/4, and 1/6 were calculated to be 81, 75, and 57 kJ/mol, respectively. Nafion has high conductivity via both the Grotthuss and vehicle mechanisms at 100% RH. At 100% RH, proton transfer in the present hybrid membrane occurs via water-cooperative conduction mechanism through the hydrophilic nanochannels. At low humidities, however, the proton transfer decreases due to the depletion of water in the nanochannels. The decrease in the water content necessary for water-assisted proton conduction is considered to increase the energy barrier for proton transfer.

Figure 22.9 shows the hybrid membrane with Si/P = 1/6 composition attached with black catalyst layers, a carbon separator, and an assembled MEA. The catalyst layer was prepared on the membrane by decal transfer method. A catalyst ink was prepared from 5% Nafion solution, Pt/C powder, and methanol. After ultrasonication, a catalyst ink was uniformly casted on a Teflon film. The catalyst layer on the Teflon film was cut into a desired size, and then hot pressed on the hybrid membrane, yielding the laminated composite film consisting of the membrane, the catalyst layer, and the Teflon film. After hot press, the Teflon film was peeled off

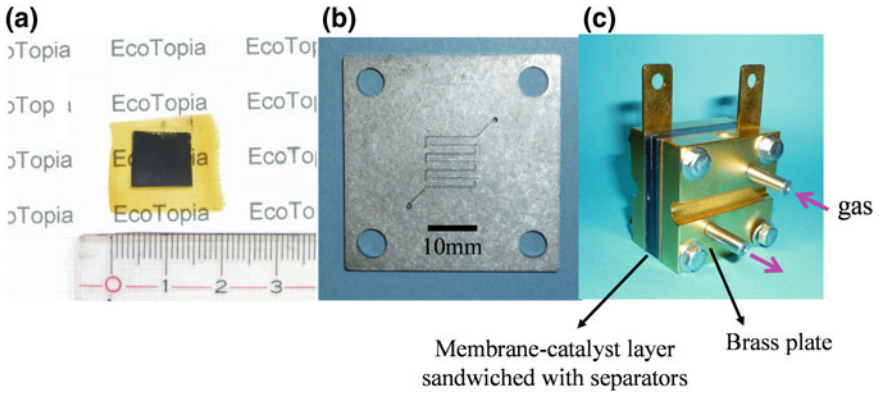

Fig. 22.9 Photographs of hybrid membrane with catalyst layers, carbon separator, and assembled MEA, **a** hybrid membrane (Si/P = 1/6) with catalyst layers, **b** carbon separator, **c** assembled MEA

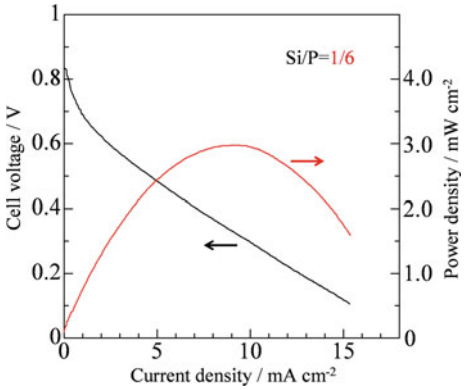

Fig. 22.10 I–V properties of the hybrid membrane of TMSMS/FC_6H_4VPA (Si/P = 1/6) measured at 140 °C and 30% RH. Reprinted from Ref. [18]. Copyright 2015, with permission from Elsevier

from the membrane–catalyst layer composite, resulting in the preparation of a membrane with catalyst layers as shown in Fig. 22.9a. The carbon separator has a serpentine flow channel for hydrated gases, such as oxygen and hydrogen (Fig. 22.9b). Hydrogen or oxygen gas is supplied to the flow channel through the tubing shown in Fig. 22.9c. The MEA was constructed from the membrane with catalyst layers sandwiched with a pair of carbon separators as shown in Fig. 22.9c. The brass plates are used as heat transfer elements from a flexible heater (not shown in Fig. 22.9c).

Figure 22.10 shows the power densities for an MEA fabricated using the hybrid membrane with Si/P = 1/6 at 30% RH. The peak power density was 3.0 mW/cm^2 at 140 °C with an open-circuit voltages (OCVs) of 0.85 V. The initial lower OCV may be due to gas cross-over or an internal micro short-circuit as the result of a reduction of the mechanical strength of the membrane at 140 °C. Although many examples of I–V properties at 100% RH below 100 °C have been reported for various membranes, not many papers deal with the cell properties at temperatures above 120 °C and low RH. The reported power densities for siloxane-based membranes are as follows: a silylmethylstyrene derivative–phosphoryl acrylate system, ~3 mW/cm^2 at 120 °C and 51% RH [11], and silylmethylmethoxystyrene derivative–methacryl phosphonic acid membrane, 4.8 mW/cm^2 at 140 °C and 30% RH [19]. The cell fabricated from the prepared hybrid membrane showed an I–V performance at an intermediate temperature and low humidity, although further investigation is required to improve the cell properties.

22.6 Conclusions

Proton-conductive inorganic–organic hybrid membranes of Class II type were synthesized from a mixture of TMSMS and FC_6H_4VPA. The formation of the inorganic–organic membranes consisting of Si–O networks and aliphatic polymer chains bound with phosphonic acid groups was confirmed based on IR and ^{29}Si

NMR. These membranes were self-standing, homogeneous, and exhibited high formability, and high thermal stability up to 180 °C. F substitution in the aromatic ring of phenylphosphonic acid was effective for the increase of the T^3 unit of the silica linkages, resulting in the increased Young's modulus of the membranes. The proton conductivities of the hybrid membranes were dependent on the phosphonic acid content, and increased with temperature up to 130 °C. MEAs were fabricated using the membranes with improved strengths. The peak power density for the MEA prepared from the TMSMS/FC_6H_4VPA membrane with a Si/P ratio of 1/6 was 3.0 mW/cm^2 at 140 °C and 30% RH. Chemical design of the monomers was found to be useful for the synthesis of hybrid membranes that work over a broad range of operating conditions from low to 100% RH at intermediate temperatures.

References

1. B.G. Pollet, I. Staffell, J.L. Shang, Electrochim. Acta **84**, 235 (2012)
2. U. Winter, H. Weidner, Fuel Cells **3**, 76 (2003)
3. M. Aparicio, A. Duran, J. Sol-Gel. Sci. Technol. **31**, 103 (2004)
4. Q. Li, R. He, J.O. Jensen, N.J. Bjerrum, Chem. Mater. **15**, 4896 (2003)
5. M.S.F. Schuster, W.H. Meyer, M. Schuster, K.D. Kreuer, Chem. Mater. **16**, 329 (2004)
6. H.W. Zhang, P.K. Shen, Chem. Rev. **112**, 2780 (2012)
7. C.L. Robert, K. Vallé, F. Pereira, C. Sanchez, Chem. Soc. Rev. **40**, 961 (2011)
8. M. Kato, S. Katayama, W. Sakamoto, T. Yogo, Electrochim. Acta **52**, 5924 (2007)
9. M. Kato, W. Sakamoto, T. Yogo, J. Membr. Sci. **303**, 43 (2007)
10. M. Kato, W. Sakamoto, T. Yogo, J. Membr. Sci. **311**, 182 (2008)
11. J. Umeda, M. Suzuki, M. Kato, M. Moriya, W. Sakamoto, T. Yogo, J. Power Source **195**, 5882 (2009)
12. Y. Xue, R. Fu, C. Wu, J.Y. Lee, T. Xu, J. Membr. Sci. **350**, 148 (2010)
13. Y. Tokuda, T. Yamada, M. Takahashi, T. Yoko, H. Kitagawa, Y. Ueda, J. Mater. Res. **26**, 796 (2011)
14. O. Sel, T. Azais, M. Maréchal, G. Gébel, C.L. Robert, C. Sanchez, Chem. Asian J. **6**, 2992 (2011)
15. U. Thanganathan, D. Dixon, S.L. Ghatty, B. Rambabu, Int. J. Hydrogen Energy **37**, 17180 (2012)
16. L. Wang, S.G. Advani, A.K. Prasad, Electrochim. Acta **105**, 530 (2013)
17. E.A. Mistri, S. Banerjee, RSC Adv. **4**, 22398 (2014)
18. M. Hattori, S. Yamaura, W. Zhang, W. Sakamoto, T. Yogo, J. Membr. Sci. **488**, 166 (2015)
19. T. Hoshino, K. Hayashi, W. Sakamoto, T. Yogo, J. Membr. Sci. **502**, 133 (2016)
20. J.F. Brinker, J. Non-Cryst. Solid **100**, 31 (1988)
21. P. Judeinstein, C. Sanchez, J. Mater. Chem. **6**, 511 (2004)
22. R.M. Silverstein, F.X. Webster, D.J. Kiemle, D.L. Bryce, in *Spectrometric Identification of Organic Compounds*, 8th edn. (Wiley, New York, 2014), p. 71
23. Y. Sugahara, S. Okada, S. Sato, K. Kuroda, C. Kato, J. Non-Cryst. Solid **167**, 21 (1994)
24. K. Miyatake, H. Zhou, T. Matsuo, H. Uchida, M. Watanabe, Macromolecules **37**, 4961 (2004)
25. X. Zhang, S. Liu, J. Yin, J. Polym. Sci. B: Polym. Phys. **44**, 665 (2006)
26. P. Innocenzi, M. Esposto, A. Maddalena, J. Sol-Gel. Sci. Technol. **20**, 293 (2001)

27. Y. Hamano, K. Yasuda, T. Yazawa, K. Kuraoka, J. Mater. Sci. **39**, 7097 (2004)
28. M. Saito, K. Hayamizu, T. Okada, J. Phys. Chem. B **109**, 3112 (2005)
29. T. Tezuka, K. Tadanaga, A. Matsuda, A. Hayashi, M. Tatsumisago, Solid State Ionics **176**, 3001 (2005)